11480 *J. Phys. Chem. A* **2001,** *105,* 11480−11487

A Comparative Classical-Quantum Study of the Photodissociation of Water in the $\tilde{B}$ Band

Rob van Harrevelt and Marc C. van Hemert*

Leiden Institute of Chemistry, Gorlaeus Laboratories, Leiden University, P.O. Box 9502,
2300 RA Leiden, The Netherlands

George C. Schatz

Department of Chemistry, Northwestern University, Evanston, Illinois 60208-3113

Received: May 15, 2001; In Final Form: October 9, 2001

A detailed comparison between three-dimensional classical surface hopping calculations and quantum mechanical calculations is presented for the photodissociation of water in the $\tilde{B}$ band. Accurate coupled diabatic potential energy surfaces are used in these calculations. Tully's "fewest switches" method using an adiabatic representation for the electronic states is applied for the surface hopping procedure. Studied are the energy dependence of the branching ratios for the possible fragmentation channels, including electronically nonadiabatic channels, and the probabilities for particular vibrational or rotational product states of the electronically excited OH(A) fragment. Although the classical results generally agree well with the quantum results, some serious errors in the classical calculations were detected. First, it is found that the calculated fractions for the $O(^1D) + H_2$ and $O(^3P) + H + H$ fragments are too large. Second, the absence of quantization of the vibrational energy in classical mechanics has consequences for the details of the rotational product state distribution of the OH(A,v=0) fragments. This is important for the "single N phenomenon", an experimentally observed strong preference for populating the highest rotational product state for which the rotational barrier energy is lower than the available energy (S. A. Harich, X. F. Yang, R. van Harrevelt, and M. C. van Hemert, *Phys. Rev. Lett.*, 2001). For a two-dimensional model, where the above-mentioned problems of classical trajectory calculations do not occur, excellent agreement between classical and quantum results is found. Classical trajectories were followed to explain the single N phenomenon and the origin of the experimentally observed vibrational excitation of OH(A) fragments.

I. Introduction

This paper concerns quasi-classical surface hopping calculations for the electronically nonadiabatic photodissociation of water in the $\tilde{B}$ band. This study has two objects. The first aim is to test the accuracy of classical results by comparing with accurate quantum mechanical results. Although classical mechanics is an approximation that is subject to zero point errors, to excessively chaotic dynamics, and to potentially important approximations in the treatment of electronically nonadiabatic effects, the classical calculations are much easier to program than quantum mechanical calculations and are in most cases computationally less demanding. Thus, if the classical description is proven to be adequate in this case, it may be used for other similar photodissociation processes.

The second purpose is to use classical mechanics to gain insight into the photodissociation dynamics. For simple processes, the expectation values of the quantum mechanical time-dependent wave packet provide a clear picture of the photodissociation dynamics. But for processes where the wave packet splits into various components, or where the dynamics is strongly energy-dependent, as is the case in the process studied in this paper, this type of an analysis of quantum dynamics is less useful. In those cases classical trajectories provide a more transparent picture of the dynamics than quantum mechanical wave packets.

There are many classical trajectory studies of photodissociation reported in the literature, with or without surface hopping: see, for example, refs 1−9. In particular, the photodissociation of water in the $\tilde{B}$ band was studied extensively with classical trajectory calculations.[1−5] At the time that these calculations were performed, an accurate three-dimensional potential energy surface for the $\tilde{B}$ state was not yet available, except for ref 5. Also, three-dimensional quantum mechanical calculations on coupled potential energy surfaces were not yet possible at that time. Only for a two-dimensional electronically adiabatic model a comparison between quantum and classical results was given.[1] Weide and Schinke[1] found good agreement between classical and quantum results for the OH(A) rotational distributions. The photodissociation of water in the $\tilde{A}$ band is much simpler because the direct photodissociation process proceeds on one single potential energy surface. Three-dimensional classical calculations, using an accurate potential energy surface for the $\tilde{A}$ state, are presented in ref 3. The classical rotational and vibrational distributions were shown to agree well with quantum results for the same surface.

The present classical surface hopping study differs from the previous studies on the following points. First, we use an accurate set of three-dimensional coupled potential energy surfaces, the Dobbyn−Knowles (DK) surfaces.[10,11] Comparisons between experimental and quantum results for OH(A) rovibrational distributions[12] indicate that this surface is better than the surfaces used in previous studies. Second, classical results are always compared with results of accurate three-dimensional

---

* Corresponding author. E-mail: hemert_m@chem.leidenuniv.nl. Fax: (+31)-71−527 4488.

10.1021/jp011871d CCC: \$20.00

quantum calculations on coupled potential energy surfaces, as discussed in ref 13. Third, we discuss quantities such as the branching ratios for different fragmentation channels, and the probability for a particular rotational or vibrational state, as a function of the photon energy. This is particularly important because quantum mechanical branching ratios and probabilities as a function of the energy usually show interference structures.

In this work, Tully's 'Fewest Switches' (TFS) algorithm[14] is used to calculate the probability of surface hops. This method is developed to minimize the number of surface hops. Since every surface hop implies an unphysically abrupt change of the momenta, the TFS method is expected to be more accurate than other surface hopping techniques. Most of the calculations use an adiabatic representation of the electronic states; however, results for diabatic states are briefly considered. As far as we know, the TFS method has not yet been applied to photodissociation, but various comparisons between the TFS and quantum results for reactive scattering are very encouraging,[15−19] and very recently, the TFS approach has been used to study quenching and reaction in OH(A) + H collision using the same potential surfaces[20] used in the study presented in this paper.

Many interesting experimental results for photodissociation of water in the $\tilde{B}$ band have recently become available. Kinetic energy release (KER) experiments have provided detailed information on the electronic and rovibrational product state distributions of OH or OD fragments from H_2O, D_2O, or HOD molecules[5] photolyzed with 121.6 nm light. These experiments revealed interesting phenomena in the rotational product state distributions of the diatomic fragments: interference structures in the rotational distributions of the OH(X,v=0) fragments from H_2O,[5] and the "single *N* phenomenon" for the OD(A,v=0) fragments from HOD.[21] In the single *N* phenomenon there is a strong preference for populating the highest possible rotational product state for which the rotational barrier energy is lower than the available energy. In another recent experimental study[12,22] the wavelength dependence of the rovibrational distribution of the OH(A)/OD(A) fragments was studied systematically, by measuring the fluorescence of the diatomic fragments. In this paper, we will use classical trajectories to study the origin of the vibrational excitation of the OH(A) fragments. We also present a classical analysis of the single *N* phenomenon.

Finally, we want to stress that some experimentally observable features are purely quantum mechanical in nature and must accordingly be described quantum-mechanically. For example, resonances in the absorption spectra,[23] which are related to Feshbach resonances on the adiabatic $\tilde{B}$ state.[24] Also, the interference pattern observed in the OH(X) rotational distribution[25] is a typical quantum phenomenon.

II. Details of the Calculations

II.A. Potential Energy Surfaces. The Dobbyn−Knowles (DK) coupled diabatic potential energy surfaces[10,11] are used in the present dynamical calculations. Adiabatic potential energy surfaces for the $\tilde{B}$ and $\tilde{X}$ states were calculated using the multireference single and double excitations configuration interaction (MRD-CI) method, with a large atomic basis set and a large number of selected configurations. The transformation from the adiabatic electronic states $\tilde{X}$ and $\tilde{B}$ to diabatic states Π and Σ was done with help of ab initio matrix elements of the electronic angular momentum operator.[10]

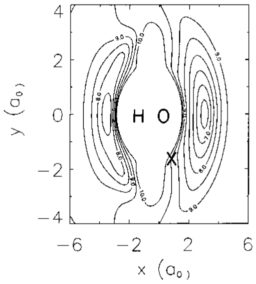

Figure 1. Dobbyn−Knowles potential energy surface for the adiabatic $\tilde{B}$ state, for a fixed OH1 distance of 1.8 a_0. The O and H1 atoms are located at (x, y) = (0.0, 0.0) and (−1.8 a_0, 0.0), respectively. Energies are in units of electronvolts; contour lines are drawn at 6.5, 7, 7.5, ..., 9.5, and 10 eV. The Franck−Condon point, where all trajectories start, is indicated with X.

In a previous study of the photodissociation of water, we used the older Leiden potential energy surfaces,[26] which were constructed in a manner similar to that for the DK surfaces. The basis set and the number of selected configurations was, however, smaller, and therefore the DK surfaces are in general more accurate than the Leiden surfaces, in particular with respect to the electronic threshold energies for various fragments (OH(X) + H, OH(A) + H, $O(^1D) + H_2$, and $O(^3P) + H + H$). For example, the DK value for the electronic threshold energy for OH(A) + H (9.42 eV), is closer to the experimental value (9.52 eV[27]) than the Leiden result (9.34 eV). Because the OH(A) + H threshold energy is within the energy range of the dissociating wave packet, the dynamics are quite sensitive to this threshold energy. Also, a comparison between quantum results with experimental data[12] for the vibrational distributions of OH(A) fragments indicates the Dobbyn−Knowles surface for the $\tilde{B}$ state is more accurate than the Leiden $\tilde{B}$ surface.

In a previous study of photodissociation of water in the $\tilde{A}$ band,[28] we have compared the DK and Leiden $\tilde{A}$ surfaces. We used a simple empirical correction function to correct the OH(X) threshold energy. Remarkably, from comparisons between theoretical and experimental OH(X) vibrational distributions, we concluded that the corrected Leiden $\tilde{A}$ surface is *more* accurate than the corrected DK $\tilde{A}$ surface, in contrast to the indication that the Leiden $\tilde{B}$ surface is *less* accurate than the DK $\tilde{B}$ surface. We have not used empirical corrections for the $\tilde{B}$ state surfaces, because the dissociation dynamics on the $\tilde{B}$ surface is significantly more complex than the dynamics on the $\tilde{A}$ surface and is therefore more sensitive to minor details of the correction function.

Besides the accuracy, an additional advantage of the DK surfaces is that they are available in analytical forms, which is convenient for classical calculations. In Figure 1, we show a two-dimensional contour plot of the potential energy surface for the adiabatic $\tilde{B}$ state, which explains the main characteristics of the photodissociation dynamics. One OH bond length is fixed at 1.8a_0. All trajectories start on the $\tilde{B}$ state at the point indicated with the cross, the Franck−Condon point. The trajectories move toward the deep well at the linear HOH region (y = 0). The HOH minimum is the conical intersection, where many trajectories hop to the ground state surface and end at OH(X) + H. Trajectories that are not transferred to the ground state, may directly go to OH(A) + H, or move toward the well at the linear HHO geometry, which is also a conical intersection.

The coupling between the adiabatic $\tilde{X}$ and $\tilde{B}$ states arises from the nonadiabatic coupling vector $g \equiv \langle \phi_X | \nabla \phi_B \rangle$, where ϕ_X and ϕ_B are Born−Oppenheimer wave functions and ∇ is the gradient operator with respect to all nuclear degrees of freedom. This coupling can be determined from the DK diabatic potential energy surfaces V_Π and V_Σ and the coupling $V_{\Pi\Sigma}$. Diagonalization of the electronic Hamiltonian in the diabatic basis results in the Born−Oppenheimer potential energy surfaces V_X and V_B. The mixing angle is defined as $\alpha = {}^1/_2 \arctan(V_{\Pi\Sigma}/|V_\Pi - V_\Sigma|)$ and is related to **g** according to $\mathbf{g} = \nabla\alpha$. Note that it is assumed that the matrix element of ∇ in the diabatic basis is zero, which is in general not true for polyatomic systems.[29]

II.B. Quasi-Classical Surface Hopping Calculations. For the quasi-classical trajectory (QCT) surface hopping calculations, the procedure as reported by Gray et al.[19] is followed. Gray et al. studied nonadiabatic effects on the $O(^1D) + H_2$ reaction on the same set of surfaces as used in the present calculations. Modifications of this procedure for photodissociation processes are described below.

In the classical calculations, Cartesian Jacobi coordinates **r** and **R** are used, where **r** is the OH vector, and **R** is the H−OH vector. In this paper we will only consider nonrotating water molecules ($J = 0$): hence all atoms remain in a fixed plane, and we have four nuclear degrees of freedom. Actually, there are only three independent degrees of freedom, due to the conservation of the component of the angular momentum perpendicular to the molecular plane, but we do not use this in the classical calculations. Three independent degrees for freedom are, for example, R, r, and γ, the magnitude of **R** and **r**, and the angle between these two vectors, respectively.

To determine the initial values of the components of **r** and **R**, and the conjugate momenta, we follow the Wigner approach.[30,31] First, we calculate variationally the ground-state vibrational wave function $\psi(R,r,\cos\gamma)$ for $J = 0$, Then this wave function is fitted to the following functional form: $\psi(R,r,\cos\gamma) = \psi_R(R)\,\psi_r(r)\,\psi_{\cos\gamma}(\cos\gamma)$, where the function ψ_x ($x = r$, R, or $\cos\gamma$) has the form: $\psi(x) = \sqrt{\alpha_x/\pi}\,\exp(-\alpha_x(x - x_e)^2)$. The momenta conjugate to r and R are denoted as p and P, respectively. The momentum space representations of the wave functions also have a Gaussian form: $\phi(p') = \sqrt{{}^1/_4\alpha_x\pi}\,\exp(-p'^2/4\alpha_x)$, where p' is P or p. The angular momentum conjugate to γ is denoted as l. The angular momentum space representation $\phi(l)$ does not have a Gaussian form. Numerical tests, however, indicate that $\phi(l)$ fluctuates around a Gaussian function of the same form as $\phi(p')$, and we therefore can make the approximation $\phi(l) \approx \sqrt{{}^1/_4\alpha_{\cos\gamma}\pi}\,\exp(-\,l^2/4\alpha_{\cos\gamma})$. Initial values of r, R, $\cos\gamma$, p, P, and l are generated with a probability given by the Wigner function P_W: $P_W(R,r,\cos\gamma,P,p,l) = \psi(R,r,\cos\gamma)^2\,\phi(P,p,l)^2$. The Box−Moller method[32] is used to generate random numbers with a Gaussian distribution. The coordinates of the nuclei, which always lie in the yz plane, are given by $r_y = 0$, $r_z = r$, $p_y = l/r$, $p_z = p$, $R_y = R\sin\gamma$, $R_z = R\cos\gamma$, $P_y = R\sin\gamma - j\cos\gamma/R$, and $P_z = R\cos\gamma + j\cos\gamma/R$. Finally, the energy of a new trajectory is calculated. The trajectory is integrated if the energy lies within a specified interval.

For some calculations, one OH bond length (r) is fixed to an arbitrary value, which reduces the complexity of the photodissociation process. This is achieved using the Lagrange multiplier method, as described in ref 33.

In accurate quantum mechanical calculations, the results should not depend on the representation, diabatic or adiabatic. The surface hopping method, however, is more a trick than a theoretical algorithm. For example, the sudden, discontinuous switch from one surface to the other is clearly an unphysical process. Furthermore, the method is justified only for transitions between degenerate electronic states. As a consequence, the success of the method critically relies on the representation of the electronic states, as was demonstrated in previous studies.[16] We performed test calculations for the photodissociation of water, and found that surface hopping in the diabatic representation completely failed in providing a realistic description, in particular with respect to product state distributions, in contrast to the good results obtained with the adiabatic representation. This is easily understood from the shapes of the potential energy surfaces. In the diabatic representation, the interaction between the diabatic states is spread out over a wide range of nuclear geometries, where the molecule has a bent geometry. Because in these regions, the diabatic states are completely different in character, a strong change in the nature of the trajectory occurs after a successful hop, which is unphysical. This may be particularly important because all trajectories start at bent geometries.

In the adiabatic representation, the interaction is more localized at the seam of the conical intersection at the linear geometry, where the adiabatic states are nearly degenerate. When surface hops occur in this region, there is no or little change in the character of the trajectory. Trajectories to OH(X) + H usually have only one single surface hop, about half of these trajectories at the collinear HOH region, and the other half at the collinear HHO region. Surface hops at the collinear HOH region are strongly localized at the conical intersection seam. Surface hops at the collinear HHO region have a wider distribution, because the $\tilde{X}$ and $\tilde{B}$ surfaces are almost degenerate in this region. About half of the trajectories to OH(A) have no surface hop at all. For the other trajectories, a hop from $\tilde{B}$ to $\tilde{X}$ is almost immediately followed by a hop back to the $\tilde{B}$ surface. Therefore, the nature of the trajectories to OH(A) + H are hardly changed by surface hopping.

Thus for the present problem an adiabatic representation of the electronic states appears necessary for a realistic description of the photodissociation dynamics. At first sight this seems to be in conflict with the usage of the diabatic representation used in previous calculations by one of us for processes involving the same set of coupled potential energy surfaces as for the photodissociation of water: the $O(^1D) + H_2 \rightarrow OH + H$ reaction,[34] and the electronic quenching of OH(A) radicals due to collisions with H,[20] but it should be taken into account that these processes are quite different from the photodissociation of water. For the $O(^1D) + H_2 \rightarrow OH + H$ reaction it was found that a diabatic representation was modestly better than the adiabatic representation in describing transitions between the same states that are considered in the present calculation. In that case the coupling was weaker in the diabatic representation due to the constraint in the reactive trajectories to near collinear HHO geometries as a result of a barrier that must be surmounted before the conical intersection is sampled. In view of these comparisons (diabatic better for linear geometries, adiabatic best for bent geometries), it is not clear whether the adiabatic or diabatic representation is preferred in the OH(A) + H collision study reported in ref 20 where all possible orientations can contribute to the electronic quenching process.

A subtle point in surface hopping methods is the constraint of energy conservation during a surface hop. To impose energy conservation, the component of the momentum parallel to the nonadiabatic coupling vector **g** is adjusted to conserve energy. When the potential energy increases during a surface hop attempt, it may occur that the projection of the momentum on the vector **g** is too small to be adjusted. This “frustrated” surface hop is always rejected during the trajectory integration. It is a common practice to reverse the component of the momentum along **g** in the case of a frustrated hop. For the present problem we found that the momentum reversal does not change the results of the surface hopping calculations significantly, as also

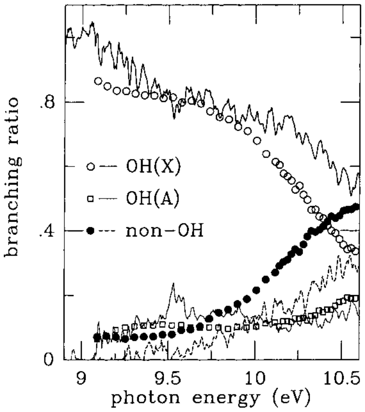

Figure 2. Branching ratios for the OH(X) + H, OH(A) + H, and non-OH + H channels, as a function of the photon energy. Solid lines are results from quantum calculations; the points are quasi-classical results.

found by Hack and Truhlar.[15] Therefore, we have not applied momentum reversal in our calculations.

When the trajectory has finished, the continuous rotational angular momentum $N_{cont} = l$ and the continuous semiclassical vibrational action v_{cont} are calculated for the OH fragment. N_{cont} is given by $N_{cont} = |r \times p|$, and $v_{cont} = -\frac{1}{2} + \oint p\, dr$, where the integration is carried out over a complete vibrational period. Note that $v_{cont} \geq -\frac{1}{2}$. The equations of ref 35 have been used in evaluating v_{cont}. To assign trajectories to discrete integer values N and v, the continuous values of N_{cont} and v_{cont} are truncated. For example, $N_{cont} = 19.7$ is assigned to $N = 19$. The advantage of truncation is that classical and quantum barrier energies are almost equal.

For the SH calculations, a time step of 1 au (0.024 fs) is used. For calculations in which the coupling between the $\tilde{B}$ and $\tilde{X}$ states is neglected, a larger time step of 5 au is sufficient.

II.C. Quantum Mechanical Wave Packet Calculations. The wave packet calculations, using a diabatic representation of the electronic states, have been described in detail in ref 13. For the analysis of the single N phenomenon, a larger grid for the R coordinate was necessary. A grid of 144 points between 1 and 15 a_0 was found to be adequate for sufficiently converged results. In contrast to the calculations in ref 13, the total angular momentum was zero in the quantum calculations presented in this paper, because the classical description is also for zero rotational angular momentum of the H_2O complex.

III. Results

III.A. Branching Ratios. Quantum and classical branching ratios for the OH(X) + H channel, the OH(A) + H channel, and the total branching ratio for the non-OH + H channels ($O(^1D) + H_2$ and $O(^3P) + H + H$) are shown in Figure 2, as functions of the photon energy. Note that the electronically nonadiabatic channel to OH(X) + H is dominant in the entire energy range. Experimentally, branching ratios are only known for a photon energy of 10.2 eV:[5] 0.66 (OH(X) + H), 0.13 (OH(A) + H), and 0.21 (other channels). The experimental branching ratios are in good agreement with the quantum results. The quantum branching ratios as presented here agree better with the experimental data than previous results reported for the Leiden surfaces,[13] for which the fraction of OH(A) fragments (0.3) is too large. The origin of the difference between the DK and Leiden results is probably a difference in the symmetric stretch potentials in the vicinity of the Franck–Condon region. For the Leiden surfaces, the initial symmetric stretch motion is more strongly excited than for the DK surfaces. This gives rise not only to excessively high vibrational excitation of the OH(A) fragments,[12] but also to a large fraction of the wave packet missing the well in the collinear HOH region. This fraction of the wave packet reaches the conical intersection seam with smaller kinetic energy, and therefore the probability of a surface hop to the ground-state surface is smaller.

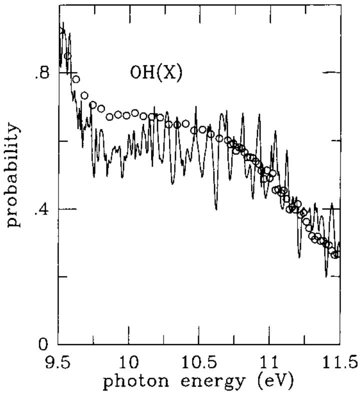

Figure 3. Branching ratio for the OH(X) channel, obtained from 2D calculations with $r = 1.8\ a_0$. Only OH(X) and OH(A) fragments are possible. Solid line: quantum results. Open circles: classical results.

The quasi-classical branching ratios agree quite well with the quantum mechanical results, except that the classical results overestimate the branching to the O + H_2 and $O(^3P) + H + H$ channels, in particular at energies above 10 eV. This can be a consequence of the surface hopping method, but quantum effects could also contribute. In a calculation in which the nonadiabatic coupling between the electronic states was switched off, only OH(A) + H and $O(^1D) + H_2$ fragments are possible. The calculated fraction of $O(^1D) + H_2$ fragments at 10.2 eV are 0.3 and 0.6 for the quantum and classical calculations, respectively. Thus, even without surface hopping, the branching to the $O(^1D) + H_2$ channel is too large, which indicates that in the classical calculations the energy flow in the triatomic complex is more efficient. The excess of the non-OH + H channels in the coupled classical treatment is probably due to the same effect.

Two-dimensional calculations in which r was fixed at 1.8 a_0 have been performed in order to test the accuracy of the surface hopping method without the complication of the presence of the non-OH + H channels. The quantum and classical probabilities for OH(X), presented in Figure 3, are in excellent agreement. This proves that the surface hopping procedure used in the present calculations is quite accurate and suggests that the deviations between the classical and quantum branching ratios for the three-dimensional case are not due to an inaccurate treatment of the nonadiabatic transitions.

In Figure 4, separate branching ratios for the $O(^1D) + H_2$ and $O(^3P) + H + H$ channels are shown. The strong increase of the non-OH channels above 10 eV is mainly due to the $O(^3P) + H + H$ channel. The trajectories to both non-OH channels almost always have their first surface hop at the collinear HHO well region. This suggests that for those trajectories that pass the collinear HHO well region, the $O(^1D) + H_2$ and $O(^3P) + H + H$ dissociation channels are competitive. However, in both the classical and the quantum calculations, the branching ratio for $O(^3P) + H + H$ is probably overestimated at the expense of the $O(^1D) + H_2$ channel, because only two electronic states ($\tilde{X}$ and $\tilde{B}$) are considered in the model. This is related to the following problem at the asymptotic H_2 + O region.

The problem is the crossing of the potential energy surfaces corresponding to $O(^1D) + H_2(X\ ^1\Sigma_g^+)$ and $O(^3P) + H_2(a\ ^3\Sigma_u^+)$.

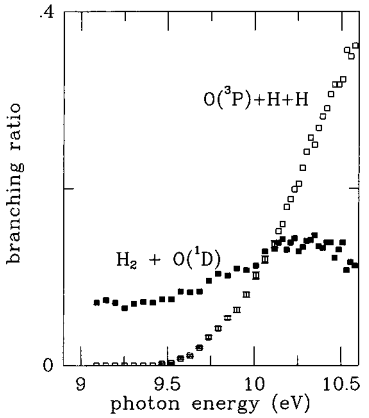

Figure 4. Classical branching ratios for the $O(^3P) + H + H$ and $O(^1D) + H_2$ channels, as functions of the photon energy.

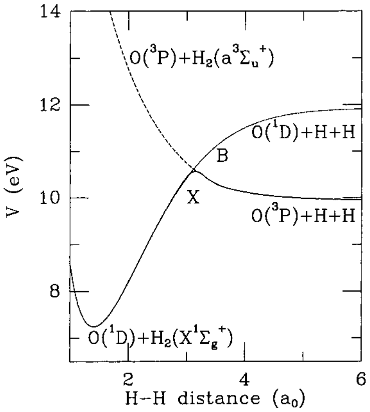

Figure 5. Dobbyn–Knowles potential energy surfaces for the adiabatic X and $\tilde{B}$ states, as functions of the H–H distance, for an infinitely far oxygen atom. Solid line: X surface. Dotted line: $\tilde{B}$ surface. A schematic potential energy curve for the repulsive a $^3\Sigma_u^+$ state of H_2, correlating with $O(^3P)$, is indicated with the broken line.

When the O atom is infinitely far apart, the potentials corresponding to these fragments cross at a H–H distance (r_{HH}) of 3.1 a_0, because the energy of $O(^3P)$ is about 2 eV lower than the energy of $O(^1D)$. This is illustrated in Figure 5. As a consequence, the ground state ($\tilde{X}$) surface has $O(^1D) + H_2$ $(X^1\Sigma_g^+)$ character for $r_{HH} < 3.1\ a_0$ and $O(^3P) + H_2(a^3\Sigma_u^+)$ character for $r_{HH} > 3.1\ a_0$ at the asymptotic region. This is clearly seen in Figure 5. The intersection at $r_{HH} = 3.1\ a_0$ should be a sharp kink, but due to the fitting of the surface with an analytical function, the sharp kink is rounded off. For the $\tilde{B}$ surface, this problem does not occur, because there is only one electronic state of A′ symmetry correlating with $O(^3P) + H + H$.

As a consequence, on the ground-state surface the following dissociation process may occur: $O(^1D) + H_2 \rightarrow O(^3P) + H + H$. For an infinite O–$H_2$ distance, this process is an artifact of the potential energy surface model, since this process can of course never occur in nature. In a correct treatment, one should include an electronic state correlating with both $O(^3P) + H_2(a^3\Sigma_u^+)$, and $O(^1D) + H + H$. This is the fifth state of A′ symmetry, or the second state of B_2 symmetry for C_{2v} geometries. The coupling between this state and the $\tilde{X}$ state, which for C_{2v} geometries also has B_2 character in the $H_2 + O$ region, should be included in this correct treatment. The complexity of such a treatment is, however, prohibitively large.

III.B. Rovibrational Distributions of the Diatomic Fragments. In general, the classical rovibrational distributions for the OH(X) and OH(A) fragments are in good agreement with the quantum results. The OH(X) rotational and vibrational distributions are hardly energy dependent. We found small deviations between quantum and classical vibrational distributions for OH(X): the quantum vibrational distribution is somewhat sharper peaked at $v = 0$. For example, at 10.2 eV, the quantum mechanical probabilities are 0.56 ($v = 0$), 0.05 ($v = 1$), 0.06 ($v = 2$), and 0.05 ($v = 3$). The corresponding classical probabilities are 0.41 ($v = -1$ and $v = 0$), 0.10 ($v = 1$), 0.07 ($v = 2$), and 0.05 ($v = 3$).

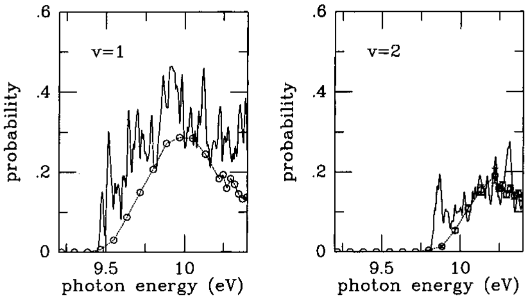

Figure 6. Vibrational product state probability for the OH(A) fragments, as a function of the photon energy, for $v = 1$ and $v = 2$. Solid lines: quantum results. Points: classical results.

The classical calculations reported in this paper confirm the picture presented by Dixon[5] for the OH(X) vibrational distribution. He showed that for those trajectories that have their first surface hop close to the collinear HOH region, the OH(X) fragments are predominantly formed with $v = 0$ and $v = 1$. In contrast, when the trajectory has the first surface hop at the collinear HHO region, the final vibrational quantum number can be very large (more than 10). The origin of the strong vibrational excitation for these trajectories is the collision between the OH fragment and the H atom.

For the OH(A) fragments, only vibrational levels with $v \leq 3$ are energetically accessible for energies below 10.4 eV. Classical and quantum probabilities for $v = 1$ and $v = 2$ are presented in Figure 6. Agreement between classical and quantum results is good. Figure 7 shows typical trajectories to OH(A,v=0) and OH(A,v=2). For the trajectory to $v = 0$, the vibrational energy increases smoothly when the trajectory moves toward the collinear HOH region. For most trajectories to $v = 2$, on the contrary, the vibrational excitation results from a OH–H collision at the collinear HHO region, the same mechanism responsible for the high vibrational excitation of the OH(X) fragments.

For the OH(X) fragments, the ratio of the $v \leq 0$ and $v = 1$ probabilities is larger than for the OH(A) fragments. This is probably because the trajectories with a large vibrational action miss the deep HOH well ($r = 1.8\ a_0$), and therefore reach the conical intersection seam with a lower kinetic energy. Since the probability of a $\tilde{B}$–$\tilde{X}$ surface hop increases with the kinetic energy, the OH(X) fragments have less vibrational action.

III.C. The Single *N* Phenomenon. In ref 21, a combined experimental and theoretical study on the single *N* phenomenon in the photodissociation of HOD at Lyman α (10.2 eV) was presented. In both the experiment and the calculations a very large probability was found (≈0.5) for the highest possible rotational state for which the rotational barrier was lower than the available energy. Rotational barriers, which arise from the $N(N + 1)/(2\mu_R R^2)$ term in the Hamiltonian, were shown to play an essential role.

The rotational barrier energies can be calculated quantum mechanically as follows. For a grid of R values, the two-dimensional Hamiltonian for the remaining degrees of freedom,

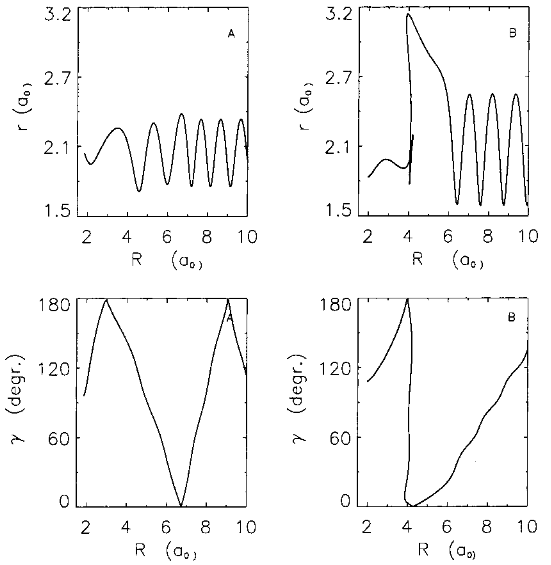

Figure 7. Two trajectories to OH(A) fragments for a photon energy of 10.2 eV. In upper panels, R and r are plotted, in the lower panels R and γ. Trajectories A and B are typical trajectories to OH(A,v=0) and OH(A,v=2), respectively.

γ and r, is diagonalized, using a Fourier grid for r and a basis set expansion in Legendre polynomials $P_l(\cos \gamma)$. The coupling between the motion for r and γ is neglected. The eigenvalues form the set of rovibrationally adiabatic potentials $V_{vN}(R)$; $V_{vN}(\infty)$ is equal to the energy of OH(v,N) + H. The adiabatic potential energy curves have barriers for sufficiently high N values. The locations of the barriers, at $R > 6\ a_0$, are far enough outside the strong interaction region to justify the approximation of decoupling motion in the R, r, and γ degrees of freedom. The barrier energies are significantly higher than the threshold energies, i.e., the asymptotic values of the $V_{vN}(R)$ curves. For example, the OH(A,v=0,N=25) threshold and barrier energies are 10.9 and 11.0 eV respectively.

Quantum wave packet calculations[21] with the Leiden potential energy surface indicate that single N phenomenon occurs at various energies around 10.2 eV for various rotational quantum numbers, not only for the OD fragments of HOD but also for the OH fragments from H_2O. An important difference between the H_2O and HOD cases is, however, that the single N phenomenon occurs at higher energies for H_2O (10.25−10.75 eV) than for HOD (10.0−10.5 eV), due to the difference in the rotational constants of OH(A) and OD(A). Therefore, an experimental detection of the single N phenomenon may be easier for HOD than for H_2O. Furthermore, at energies higher than 10.2 eV the effect of higher electronic states than the $\tilde{B}$ state may complicate the photodissociation dynamics.

In the previous study[21] we used the Leiden surface. New calculations with the DK surface confirm the picture obtained from calculations with the Leiden surface, both for HOD and H_2O. In this paper we present DK results for H_2O, both for a full three-dimensional (3D) and a two-dimensional (2D) treatment in which r was fixed at 1.8 a_0. In the following, we discuss the energy and N dependence of the $P_N(E)$ function, i.e., the probability that the OH(A,v=0) fragment has rotational angular momentum N for a total energy E. The total energy is the photon energy plus the zero point vibrational energy of H_2O (0.57 eV for the 3D case).

Before presenting the classical results for the $P_N(E)$ function, we first discuss the quantum results. The quantum result for $P_{25}(E)$ as a function of the energy is presented in the left panel in Figure 8. We chose $N = 25$, because the maximum of $P_N(E)$ is largest for this N value. The quantum $P_N(E)$ function rises rapidly with the energy above the barrier energy, but decreases again above the barrier energy corresponding to $N = 26$. Consequently, the P_{25} function has a maximum at an energy between the barriers for $N = 25$ and 26. At this energy (11.01 eV), the rotational population distribution is strongly peaked at $N = 25$: in other words, we observe the single N phenomenon. This is illustrated in the right panel of Figure 8, where $P_N(E{=}11.01\ \text{eV})$ is plotted as a function of N.

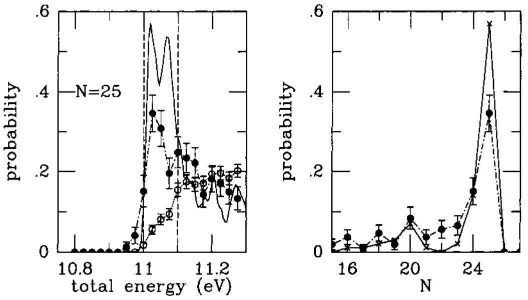

Figure 8. Left panel: P_{25} as a function of the total energy (photon energy plus zero point vibrational energy). Solid line: quantum result. Open circles: standard classical trajectory results. Closed circles: classical trajectory result for a v_{cont} interval of −0.05 to +0.05. The vertical dashed lines indicate barrier energies for $N = 25$ and $N = 26$. Right panel: $P_N(E)$ as a function of N, for $E = 11.02$ eV. Crosses: quantum results. Closed circles: classical trajectory result for a v_{cont} interval of −0.05 to +0.05.

The classical $P_{25}(E)$ function is included in Figure 8 (open circles). Deviations between classical and quantum results, clearly visible in this figure, are due to the averaging over v_{cont} between 0 and 1 for the classical results. A very simple solution to this problem is to only consider trajectories for which the continuous vibrational action v_{cont} lies in a small interval around $v_{\text{cont}} = 0$, e.g., $-0.05 \leq v_{\text{cont}} \leq 0.05$. The P_N function for this v_{cont} interval is included the left panel of Figure 8 and is in excellent agreement with the quantum result. This function still has a lower maximum than the quantum function, because of the averaging over N_{cont} between 25 and 26, and because the quantum function shows an interference structure, which enhances the maximum probability.

In the right panel of Figure 8, the classical rotational distributions for v_{cont} intervals of −0.05 to +0.05 are included, for energies where the P_{25} function has a maximum (11.02 eV). The single N phenomenon is reproduced by the classical calculations for v_{cont} interval of −0.05 to +0.05, but not for the standard interval 0−1. For the standard vibrational action interval, the maximum of the P_N function disappears in the process of averaging over v_{cont}, because the maximum of the P_N function shifts to higher energies with increasing v_{cont}. For example, for a v_{cont} interval of 0.4−0.5, the maximum has shifted to 11.22 eV.

For trajectories with v_{cont} between −0.05 and +0.05, we found good agreement between quantum and classical results. We therefore conclude that the single N phenomenon can be described classically. However, because we throw away many trajectories with v_{cont} outside the selected interval, a large amount of trajectories, about 200 000, must be calculated for statistically accurate results for the $P_N(E)$ function. The required computer time is then comparable to the computer time for a quantum calculation. Therefore, the narrow vibrational action interval procedure is not suitable for practical applications.

In the two-dimensional model, where r is fixed at 1.8 a_0, the OH vibration problem does not occur. Therefore, the quantum and classical P_{24} functions, presented in Figure 9, agree well.

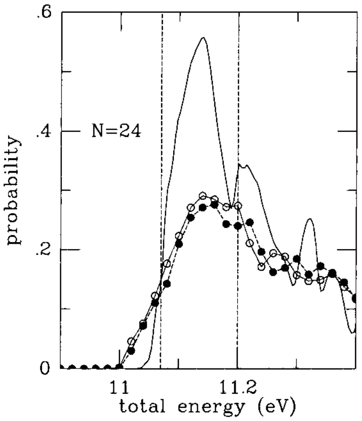

Figure 9. P_{24} as a function of the total energy (photon energy plus zero point vibrational energy), obtained from two-dimensional calculations. Solid line: quantum result. Open circles: classical results with surface hopping. Closed circles: classical results without surface hopping.

Results of classical calculations in which the coupling between the electronic states was neglected, included in Figure 9, agree very well with the fully coupled results. Since the main features of the single *N* phenomenon are also found in the two-dimensional single surface model, this simplified model is used to study the mechanism of the single *N* phenomenon.

In a previous paper[21] we have interpreted the single *N* phenomenon in terms of dynamically constraint trajectories, i.e., trajectories that have turning points in the dissociation coordinate *R* due to the rotational barrier. We have argued that this leads to a preference for the highest final *N* value for which the barrier is below the available energy. The classical calculations confirm this picture and make it possible to study this mechanism in more detail than is possible in a quantum mechanical study. We have followed single surface trajectories for the 2D model, in which r was fixed at 1.8 a_0. The energy of the trajectories was chosen in a bin of 11.1−11.2 eV, where the rotational distribution shows a single *N* phenomenon for $N = 24$. Three typical trajectories are shown in Figure 10. In the panels on the left, *R* and γ during a trajectory are plotted, and on the panels on the right, *R* and the rotational angular momentum *N*. The trajectories first go to the region of the collinear HOH well, where the rotational angular momentum reaches a maximum. When the trajectories go to the other collinear region (HHO), *N* initially decreases because the potential energy increases with decreasing HOH bond angle, but after $\gamma = 50°$, the potential decreases again. Depending on the *R* value at which the trajectory passes the collinear HHO region, R_{HHO}, the rotational angular momentum reaches a second maximum when the trajectory arrives at the collinear HHO region. The increase of *N* is larger for trajectories with lower R_{HHO} values. For trajectory A ($R_{\mathrm{HHO}} = 4.7$ a_0), *N* increases to such an extent that the rotational barrier prevents direct dissociation, and the motion in *R* has a turning point. For trajectory B, R_{HHO} is a larger, and although *N* has a maximum at the collinear HHO region, the rotational barrier is low enough. This trajectory ends at the single *N* ($N = 24$). No substantial increase of rotational angular momentum occurs when trajectory C approaches the collinear HHO region, since R_{HHO} is quite large (7.3 a_0).

The trajectories can be divided into three types, depending on the value of *R* at which the trajectories pass the collinear HHO region for the first time: those with $R < 5.5$ a_0 (A), with 5.5 $a_0 \leq R \leq 6.5$ a_0 (B), and with $R > 6.5$ a_0 (C). The three trajectories in Figure 10 are typical examples of the three types of trajectories. Type A trajectories are always indirect. We now label the trajectories not only with the final angular momentum *N*, but also with the type of the trajectory. Probabilities for a rotational state *N* and a particular type T (T = A, B, C), are presented in Figure 11, for an energy bin 11.1−11.2 eV. The rotational distributions for type A and type C trajectories are strongly inverted but do not show the single *N* phenomenon. In contrast, the rotational distribution for type B trajectories shows an extreme single *N* phenomenon. We therefore conclude that the single *N* phenomenon originates from type B trajectories, i.e., trajectories that pass the collinear HHO region with the *R* values low enough to produce a visible increase in *N*, without being trapped due to the rotational barrier.

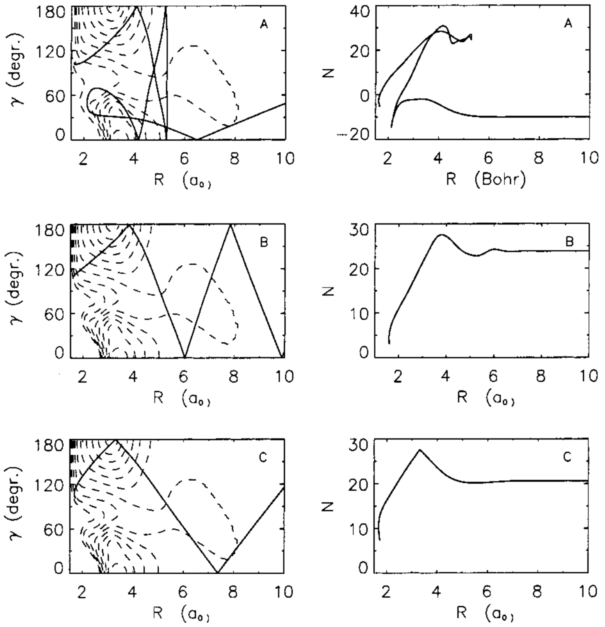

Figure 10. Three typical single surface trajectories for the 2D model. On the panels on the left, γ and *R* are plotted, on the panels on the right, *N* and *R*. The labels of the trajectories (A, B, and C) correlate with the three types of trajectories, as discussed in the text. A contour of the 2D potential is indicated in the panels on the left. The contours are for energies between 11.5 and 6.5 eV, with an energy difference of 0.5 between each contour line.

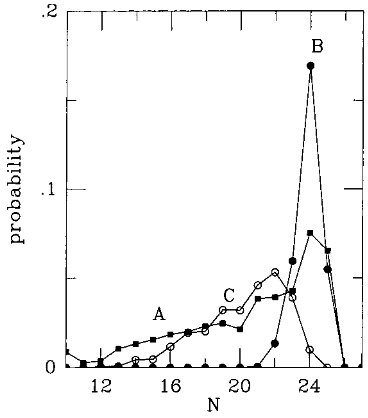

Figure 11. Probability for the trajectory to have type T (A, B, or C) and end with a rotational quantum number *N*, as a function of *N*. The types of the trajectories are discussed in the text. The energy bin was 11.1−11.2 eV.

III.D. Comparison with the OH(A) + H Collision Process. It is interesting to compare the photodissociaton process discussed in this paper with scattering of OH(A) on H, since both processes occur on the same set of coupled potential energy surfaces. A quasi-classical trajectory study of collision of OH(A) with H has been reported recently.[20] To compare photodissociation with the collision process, we performed OH(A) + H calculations for zero impact parameter, corresponding to a zero overall rotation of the complex, for a H−OH translational energy of 0.09 eV (2 kcal/mol). The calculated OH(X) + H/OH(A) + H/O(^{1}D) + H_2 branching of 0.78/0.07/0.15 is close to the branching for the photodissociation process at 9.2 eV (see Figure 2). This is surprising, since the photodissociation and the collision processes are quite different, as is evident from the large difference between the OH(X) product vibrational and rotational population distributions. For photodissociation, the vibrational distribution is sharply peaked at peaked at $v = 0$. In contrast, the vibrational population distribution of the OH(X) fragments from the collision is much broader. The rotational distribution of the OH(X,v=0) fragments from photodissociation is strongly inverted, with a maximum at $N = 38$, while the OH(X,v=0) rotational distribution for the collision has a maximum at $N = 0$. The main difference between the photodissociation and the OH(A) + H collision is that for photodissociation all trajectories start at a bent geometry, whereas in the collision the initial angle between the OH(A) molecule and the H atom can have any value, with equal probability (see Figure 1). OH(X) fragments formed after a collision of OH(A) with H in a near-collinear arrangement (HOH or HHO) have a low rotational angular momentum. Highly rotationally excited fragments can only be produced for those collisions for which the H atom attacks OH in the perpendicular direction.

IV. Conclusions

The first purpose of this work was to test the accuracy of classical surface hopping calculations for an electronically nonadiabatic process. Detailed comparisons between classical and quantum branching ratios and OH(A) rovibrational distributions for a wide range of energies have been discussed in this paper. The rovibrational distribution of the OH(X) fragments are not discussed here, because our classical calculations confirm the results obtained by Dixon[21] for a photon energy of 10.2 eV and because the OH(X) rovibrational distribution is hardly energy dependent.

The classical results agree quite well with the quantum results, provided that an adiabatic representation of the electronic states was used. However, we found some inadequacies of the classical calculations. The classical fraction of non-OH channels was too large for energies above 10 eV, which is probably due to a more efficient energy flow in the triatomic complex. Another problem is that for studying subtle effects in the rotational distribution, such as the single N phenomenon, the absence of the quantization of the vibrational action and of the zero point vibration in classical mechanics is a serious problem.

For the 2D model, in which r was fixed at 1.8 a_0, the above-mentioned problems do not exist: non-OH channels are impossible, and the vibrational action problem for the OH(A,v=0) rotational distribution does not occur. Consequently, for the 2D model we obtained excellent agreement between quantum and classical results, both for the branching ratio and the single N phenomenon.

The second purpose of classical calculations is to help with the interpretation of quantum results. For this purpose, the classical calculations do not need to be accurate. The classical calculations indicate that the strong vibrational excitation of OH(A) results from OH−H collisions at the collinear HHO geometry. Classical calculations also help to understand better the single N phenomenon. The single N phenomenon can be reproduced with classical trajectory calculations, both for the two-dimensional model and for the three-dimensional system with a small vibrational action interval. An analysis of 2D trajectories indicates that the trajectories leading to the single N are those trajectories that pass the collinear HHO region with just the right R value for an optimal increase of the angular momentum without the trajectory being trapped due to too high a rotational barrier.

Our final conclusion is that for photodissociation processes classical results do not always agree quantitatively with quantum results. In the absence of quantum results, the classical results should be handled with skepticism. But a classical treatment is realistic enough to mimic the qualitative aspects of the photodissociation process. Classical calculations accompanying quantum calculations will always increase the insight into the dynamics.

Acknowledgment. We thank Professor P. J. Knowles for making available the Dobbyn−Knowles potential energy surfaces and Professor E. F. van Dishoeck for valuable comments on the manuscript.

References and Notes

(1) Weide, K.; Schinke, R. *J. Chem. Phys.* **1987**, *87*, 4627.
(2) Dunne, L. J.; Guo, H.; Murrell, J. N. *Mol. Phys.* **1987**, *62*, 283.
(3) Guo, H.; Murrell, J. N. *J. Chem. Soc., Faraday Trans. 2* **1988**, *84*, 949.
(4) Heumann, B.; Kühl, K.; Weide, K.; Düren, R.; Hess, B.; Meier, U.; Peyerimhoff, S. D. *Chem. Phys. Lett.* **1990**, *166*, 385.
(5) Harich, S. A.; Hwang, D. W. H.; Yang, X. F.; Lin, J. J.; Yang, X. M.; Dixon, R. N. *J. Chem. Phys.* **2000**, *113*, 10073.
(6) Wang, Y.; Qian, C. X. W. *J. Chem. Phys.* **1994**, *100*, 2707.
(7) Amatatsu, Y.; Yabushita, S.; Morokuma. K. *J. Chem. Phys.* **1996**, *104*, 9783.
(8) Schinke, R. *J. Chem. Phys.* **1986**, *85*, 5049.
(9) Guo, H.; Schatz, G. C. *J. Chem. Phys.* **1990**, *92*, 1634.
(10) Dobbyn. A. J.; Knowles, P. J. *Mol. Phys.* **1997**, *91*, 1107.
(11) Dobbyn, A. J.; Knowles, P. J. Unpublished work.
(12) Zanganeh, A. H.; Fillion, J. H.; Ruiz, J.; Castillejo, M.; Lemaire, J. L.; Shafizadeh, N.; Rostas, F.; Van Harrevelt, R.; Van Hemert, M. C. *J. Phys. Chem. A*, in print.
(13) Van Harrevelt, R.; Van Hemert, M. C. *J. Chem. Phys.* **2000**, *112*, 5787.
(14) Tully, J. C. *J. Chem. Phys.* **1990**, *93*, 1061.
(15) Hack, M. D.; Truhlar, D. G. *J. Phys. Chem. A* **2000**, *104*, 7917.
(16) Hack, M. D.; Jasper, A. W.; Volobuev, Y. L.; Schwenke, D. W.; Truhlar, D. G. *J. Phys. Chem. A* **2000**, *104*, 217.
(17) Topaler, M. S.; Hack, M. D.; Allison, T. C.; Liu, Y. P.; Mielke, S. L.; Schwenke, D. W.; Truhlar, D. G. *J. Chem. Phys.* **1997**, *106*, 8699.
(18) Topaler, M. S.; Allison, T. C.; Schwenke, D. W.; Truhlar, D. G. *J. Phys. Chem. A* **1998**, *102*, 1666.
(19) Gray, S. K.; Balint-Kurti, G. G.; Schatz, G. C.; Lin, J. J.; Liu, X.; Harich, S.; Yang, X. *J. Chem. Phys.* **2000**, *113*, 7330.
(20) Schatz, G. C.; Fisher, B.; Grande, W.; Kumayama, K.; Pederson, L. A. *J. Phys. Chem. A* **2001**, *105*, 2515.
(21) Harich, S. A.; Yang, X. F.; Yang, X.; Van Harrevelt, R.; Van Hemert, M. C. *Phys. Rev. Lett.*, in print.
(22) Zanganeh, A. H.; Fillion, J. H.; Ruiz, J.; Castillejo, M.; Lemaire, J. L.; Shafizadeh, N.; Rostas, F. *J. Chem. Phys.* **2000**, *112*, 5660.
(23) Wang, H. T.; Felps, W. S.; McGlynn, S. P. *J. Chem. Phys.* **1977**, *67*, 2614.
(24) Von Dirke, M.; Heumann, B.; Kühl, K.; Schröder, T.; Schinke, R. *J. Chem. Phys.* **1994**, *101*, 2051.
(25) Dixon, R. N.; Hwang, D. W. H.; Yang, X. F.; Harich, S.; Lin, J. J.; Yang, X. *Science* **1999**, *285*, 1249.
(26) Van Harrevelt, R.; Van Hemert, M. C. *J. Chem. Phys.* **2000**, *112*, 5777.
(27) Murrell, J. N.; Carter, S.; Mills, I. M.; Guest, M. F. *Mol. Phys.* **1981**, *42*, 605.
(28) Van Harrevelt, R.; Van Hemert, M. C. *J. Chem. Phys.* **2001**, *114*, 9453.
(29) Baer, M. *Chem. Phys. Lett.* **2000**, *322*, 520.
(30) Heller, E. J. *J. Chem. Phys.* **1978**, *68*, 2066.
(31) Wigner, E. *Phys. Rev.* **1932**, *40*, 749.
(32) *Numerical Recipes in Fortran 77*: *The Art of Scientific Computing*; Cambridge University Press: Cambridge, U.K., 1986.
(33) La Budde, R. A.; Bernstein, R. B. *J. Chem. Phys.* **1971**, *55*, 5499.
(34) Gray, S. K.; Petrongolo, C.; Drukker, K.; Schatz, G. C. *J. Phys. Chem. A* **1999**, *103*, 9448.
(35) Porter, R. N.; Raff, L. M.; Miller, W. H. *J. Chem. Phys.* **1975**, *63*, 2214.